Nanomaterials Hot Paper

How to cite:
International Edition: doi.org/10.1002/anie.202115747
German Edition: doi.org/10.1002/ange.202115747

# Site-Specific Reduction-Induced Hydrogenation of a Helical Bilayer Nanographene with K and Rb Metals: Electron Multiaddition and Selective $Rb^+$ Complexation

*Zheng Zhou, Jesús M. Fernández-García, Yikun Zhu, Paul J. Evans, Rafael Rodríguez, Jeanne Crassous, Zheng Wei, Israel Fernández,* Marina A. Petrukhina,* and Nazario Martín**

*Dedicated to Professor Carlos Seoane on the occasion of his 70th birthday*

***Abstract:*** *The chemical reduction of π-conjugated bilayer nanographene* ***1*** *($C_{138}H_{120}$) with K and Rb in the presence of 18-crown-6 affords $[K^+(18\text{-crown-}6)(THF)_2][\{K^+(18\text{-crown-}6)\}_2(THF)_{0.5}][C_{138}H_{122}^{3-}]$ (**2**) and $[Rb^+(18\text{-crown-}6)_2][\{Rb^+(18\text{-crown-}6)\}_2(C_{138}H_{122}^{3-})]$ (**3**). Whereas $K^+$ cations are fully solvent-separated from the trianionic core thus affording a "naked"* $\mathbf{1}^{\bullet 3-}$ *anion, $Rb^+$ cations are coordinated to the negatively charged layers of* $\mathbf{1}^{\bullet 3-}$*. According to DFT calculations, the localization of the first two electrons in the helicene moiety leads to an unprecedented site-specific hydrogenation process at the carbon atoms located on the edge of the helicene backbone. This uncommon reduction-induced site-specific hydrogenation provokes dramatic changes in the (electronic) structure of* ***1*** *as the helicene backbone becomes more compressed and twisted upon chemical reduction, which results in a clear slippage of the bilayers.*

## Introduction

With the advent of graphene in 2004,[1] a new field of study on 2D materials started involving initially carbon but, later, other elements of the Periodic Table.[2] Despite the variety of amazing properties exhibited by graphene,[3] the zero band-gap prevents its use in the search for optoelectronic properties.[4] A variety of chemical and physical methods has been developed for opening the gap with great success, namely chemical modification and/or quantum confinement, thus affording graphene derivatives and the so-called carbon nanoribbons,[5] nanographenes (NGs)[6] and graphene quantum dots (GQDs),[7] respectively.

An alternative and more recent approach to the aforementioned carbon nanoforms is the preparation of synthetic nanographenes where the tools of organic synthesis allow to prepare, in a controlled manner, a great variety of molecular nanographenes showing different sizes and shapes.[8] Furthermore, currently there is a lot of interest in preparing defined nanographenes with control on their chemical, optoelectronic, and chiroptical properties.[9] In this regard, molecular NGs have proven their interest in a variety of fields, spanning from molecular electronics[10] or photovoltaics[11] to alkali metals storage[12] and sensing,[13] to name a few.

In our research group, we have carried out the synthesis of chiral molecular nanographenes exhibiting interesting photophysical properties. In this regard, we recently reported an unprecedented helical bilayer nanographene **1** ($C_{138}H_{120}$) in which two hexa-*peri*-hexabenzocoronenes (HBC) are conjugated through a π-extended [6]-helicene moiety (Figure 1).[14]

Bilayer nanographenes are basically unknown compounds and the presence of a rigid helicene connecting the two HBC layers allows them to stack in an AA arrangement with carbon atoms centered over each other in opposite

[*] Dr. Z. Zhou, Y. Zhu, Dr. Z. Wei, Prof. Dr. M. A. Petrukhina
Department of Chemistry
University at Albany, State University of New York
Albany, NY 12222 (USA)
E-mail: mpetrukhina@albany.edu
Dr. Z. Zhou
School of Materials Science and Engineering
Tongji University, 4800 Cao'an Road, Shanghai 201804 (China)
Dr. J. M. Fernández-García, Dr. P. J. Evans, Dr. I. Fernández, Prof. Dr. N. Martín
Departamento de Química Orgánica I
Facultad de Ciencias Químicas
Universidad Complutense de Madrid
Ciudad Universitaria s/n 28040 Madrid (Spain)
E-mail: israel@ucm.es
nazmar@ucm.es
Homepage: www.nazariomartingroup.com
Dr. R. Rodríguez, Dr. J. Crassous
Institut des Sciences Chimiques de Rennes
UMR 6226 CNRS—Univ. Rennes
Campus de Beaulieu 35042 Rennes Cedex (France)
Prof. Dr. N. Martín
IMDEA-Nanociencia
Campus de la Universidad Autónoma de Madrid
C/Faraday, 9, 28049 Madrid (Spain)

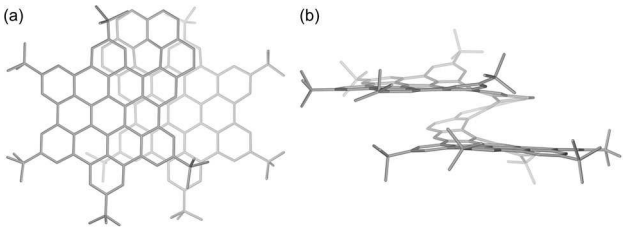


***Figure 1.*** Crystal structure of bilayer **1**: offset top view (a), side view (b). Structures shown as the *M* isomer with solvent and H-atoms excluded for clarity.

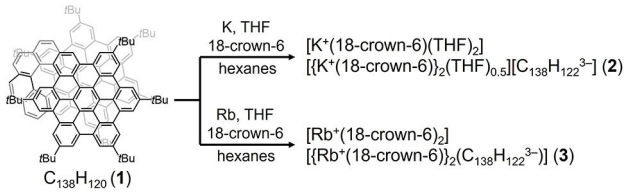


***Scheme 1.*** Chemical reduction of **1** with K and Rb metals.

layers.[15] This arrangement is different from the AB disposition found in crystalline graphite and has shown interesting crystallographic properties.

Bilayer graphene, the two-layer homologue of graphene, has recently received a lot of attention due to its singular properties. Thus, two-layer graphene has externally-tunable electronic properties different from its single-layer, namely band-gap,[16] spin-orbit interaction[17] and exciton energies.[18] Furthermore, several devices exploiting these properties have been reported.[19] Interestingly, unconventional superconductivity in magic-angle graphene superlattices has also been reported in twisted bilayer graphene.[20]

Bilayer graphene also shows facile intercalation of alkali metals. Recently, a bilayer graphene system exhibited a lithium diffusion coefficient ($7\times10^{-5}\,cm^2s^{-1}$) ten times faster than graphite, thus showing its potential as ion transport material for energy storage. Furthermore, it has been reported that the intercalation of lithium into bilayer graphene points to the existence of distinct storage arrangements of ions in 2D-layered materials as compared to their bulk parent compounds.[21]

Considering the successful aforementioned intercalation studies of bilayer graphene with lithium, we feel that molecular bilayer nanographene **1** is a highly appealing system to carry out complexation and reactivity studies with different alkali metals. Thus, in this work, we have carried out the chemical reduction of molecular bilayer graphene **1** with K and Rb metals in THF. Two products have been isolated and characterized by single crystal X-ray diffraction revealing site-specific hydrogenation of the helicene core and formation of a less-common radical trianion. In order to have a better understanding of the reduction-induced hydrogenation of helical bilayer nanographene **1**, density functional theory (DFT) calculations have also been carried out, which nicely underpin the experimental findings.

## *Results and Discussion*

The chemical reduction of **1** ($C_{138}H_{120}$) was investigated with K and Rb metals in anhydrous THF at room temperature. The reactions very quickly (within 20–30 minutes) proceed to afford dark brown solutions, which upon slow diffusion of hexanes in the presence of 18-crown-6 produce the corresponding single crystals (Scheme 1). Their X-ray diffraction analyses confirmed the formation of a solvent-separated ion product (SSIP) with potassium counterions, $[K^+(18\text{-crown-}6)(THF)_2][\{K^+(18\text{-crown-}6)\}_2(THF)_{0.5}][C_{138}H_{122}{}^{3-}]$ (**2**, crystallized with ten interstitial hexanes molecules as $\mathbf{2}\cdot10\,C_6H_{14}$), and a contact-ion complex with rubidium counterions, $[Rb^+(18\text{-crown-}6)_2][\{Rb^+(18\text{-crown-}6)\}_2(C_{138}H_{122}{}^{3-})]$ (**3**, crystallized with four interstitial THF molecules as $\mathbf{3}\cdot4\,THF$).

Notably, according to the structural analysis, the elongation of two C–C bonds is observed on the edge of the helicene backbone in both **2** and **3** compared with **1**: 1.395(11)–1.411(12) Å in **1**, 1.494(12)–1.518(12) Å in **2**, and 1.451(11)–1.474(11) Å in **3**. The bond angles on these two C-atoms in **2** and **3** are also reduced compared to those in **1** (121.6°/121.9° in **1**, 115.0°/116.4° in **2**, and 116.7°/117.2° in **3**). Both parameters indicate the double hydrogenation of the trianionic helicene core, which was further confirmed by the localization of two H-atoms on these two C-atoms in the difference Fourier map during structural refinement (see the Supporting Information for more details). The specific six-membered rings at the helicene backbone show significant deviation from planarity due to inherent strain in parent **1**,[14] so these sites revealed a high propensity for hydrogenation upon reduction, resulting in the formation of a new bilayer graphene anion, $C_{138}H_{122}{}^{3-}$ (Figure 2). To the best of our knowledge, such strain-induced reactivity of the helicene backbone has not been reported so far. However, the hydrogenation process seems related to the unsuccessful synthesis of highly curved polycyclic carbon nanobelts by reductive aromatization which gave hydrogenated products.[22]

In the crystal structure of **2** (Figure 3), the $[K^+(18\text{-crown-}6)(THF)_2]$ and $[K^+\{(18\text{-crown-}6)\}_2(THF)_{0.5}]$ moieties are solvent-separated from the trianionic core affording a "naked" $C_{138}H_{122}{}^{3-}$ anion. The K1 ion is equatorially bound to one 18-crown-6 ether ($K–O_{crown}$: 2.73(3)–2.87(3) Å) and capped by two THF molecules ($K–O_{THF}$: 2.60(3)/2.87(3) Å); while the K2 and K3 ions are hexacoordinated by one 18-

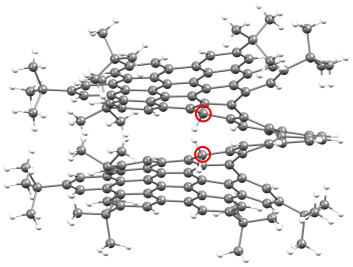

***Figure 2.*** The core of $C_{138}H_{122}{}^{3-}$ in **2** and **3**, ball-and-stick model.

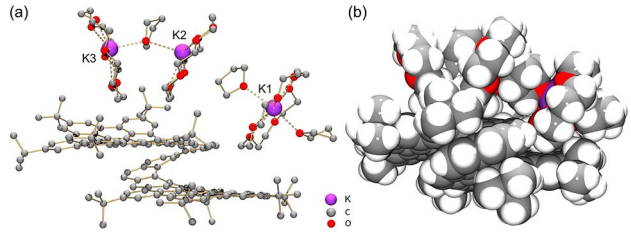


***Figure 3.*** Crystal structure of **2**, ball-and-stick (H-atoms are omitted) and space-filling models.[24]

crown-6 ether each ($K–O_{crown}$: 2.778(9)–2.931(10) Å and 2.46(4)–3.23(7) Å) and are also bridged by a THF molecule ($K–O_{THF}$: 2.69(7)/2.97(3) Å). All $K–O_{crown}$ and $K–O_{THF}$ distances are comparable to those previously reported.[23]

In the crystal structure of **3** (Figure 4), the Rb1 and Rb2 ions are coordinated to the central six-membered rings of the bilayer helicene in the $\eta^3$-mode (Figure 5). The Rb–C distances of 3.245(8)–3.390(8) Å and 3.132(8)–3.414(7) Å, respectively, are close to those reported in the literature.[25]

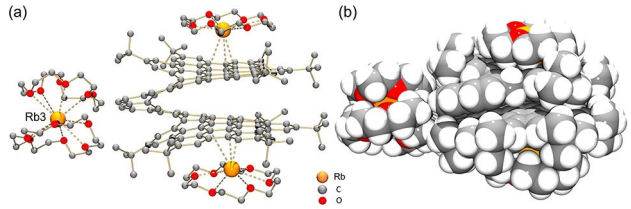


***Figure 4.*** Crystal structure of **3**, ball-and-stick (no H-atoms) and space-filling models.[24]

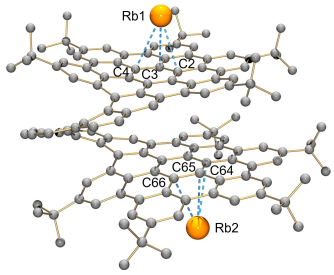


| Bond | Distance |
|---|---|
| Rb1–C2 | 3.470(11) |
| Rb1–C3 | 3.245(10) |
| Rb1–C4 | 3.390(11) |
| Rb2–C64 | 3.261(7) |
| Rb2–C65 | 3.132(8) |
| Rb2–C66 | 3.414(7) |

***Figure 5.*** Coordination of $Rb^+$ ions in the $[\{Rb^+(18\text{-crown-}6)\}_2(C_{138}H_{122}{}^{3-})]^-$ anion in **3** (H-atoms and 18-crown-6 are omitted).

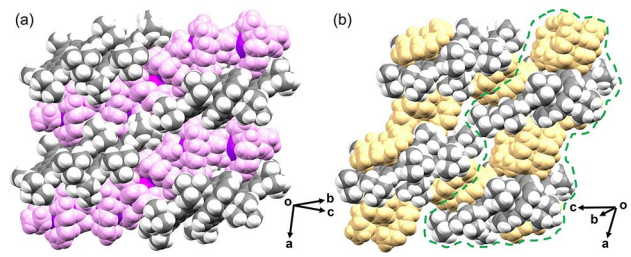


***Figure 6.*** Solid-state packing in a) **2** and b) **3**, space-filling models. $\{K^+(18\text{-crown-}6)(THF)_n\}$ moieties are shown in purple, and $\{Rb^+(18\text{-crown-}6)_n\}$ moieties are shown in yellow.

The coordination environment of these $Rb^+$ ions is completed by an 18-crown-6 ether ($Rb–O_{crown}$: 2.411(6)–3.306(6) Å). In contrast, the Rb3 ion is fully wrapped by two 18-crown-6 ether molecules ($Rb–O_{crown}$: 2.964(6)–3.466(6) Å) and remains solvent-separated from the complexed $[\{Rb^+(18\text{-crown-}6)\}_2(C_{138}H_{122}{}^{3-})]^-$ anion. All $Rb–O_{crown}$ distances are consistent with those previously reported.[25,26]

In the solid-state structure of **2** (Figure 6a), an extended 2D layer is formed through C–H···π interactions between the $C_{138}H_{122}{}^{3-}$ anions and the $\{K^+(18\text{-crown-}6)(THF)_n\}$ moieties, with the shortest contacts ranging from 2.355(12) Å to 2.713(12) Å. In **3**, the 1D columns (highlighted by the green circle, Figure 6b) are formed through C–H···π interactions (2.563(13)–2.722(13) Å) between the $C_{138}H_{122}{}^{3-}$ anions and the $\{Rb^+(18\text{-crown-}6)_2\}$ moieties. No significant interactions are found between adjacent layers in **2** or adjacent columns in **3**.

In-depth crystallographic analysis reveals a structural deformation of the helical bilayer framework upon reduction. The selected interlayer distance is reduced from 3.774 Å in neutral **1** to 3.707 Å in the new trianion of **2**, and further down to 3.603 Å in **3** (Table 1). The compression is also accompanied by the slippage of the two HBC layers. The slip distance of 0.434 Å in **1** is increased to 0.884 Å and 0.744 Å in the doubly hydrogenated trianions in **2** and **3**, respectively. Thus, the helicene backbone becomes more compressed and twisted upon chemical reduction, which is consistent with the structural response of the stepwise reduced double[7]helicene.[25b]

It could be noted that the reduction of **1** is accompanied by the geometry change of the framework which can be reflected by comparing the dihedral angles in the new doubly-hydrogenated trianion of **2** and **3** vs. those in parent **1**. The dihedral angle ∠A/B of 19.8° in **1** gradually decreases to 11.5° in **2** and 9.2° in **3** (see Table S4 for ring labels and more details), which indicates the strain reduction between the helicene backbone and the HBC layer. Moreover, the addition of electrons leads to an increase of nonplanarity in the HBC layer as can be seen from comparison of selected dihedral angles in the "naked" trianion in **2** with to those in **1**. In contrast to **2**, the corresponding dihedral angles are reduced in **3**, stemming from capping the HBC layers with two coordinated $\{Rb^+(18\text{-crown-}6)\}$ moieties.

***Table 1:*** Interlayer (the two benzene rings from the edge) and slip distances [Å] in **1** and $C_{138}H_{122}{}^{3-}$ in **2** and **3**.

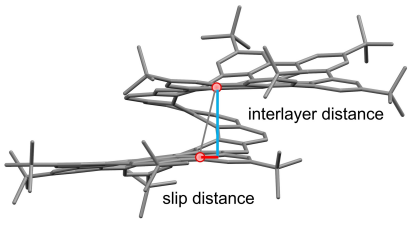


| | **1**[14] | **2** | **3** |
|---|---|---|---|
| Interlayer distance | 3.774 | 3.707 | 3.603 |
| Slip distance | 0.434 | 0.884 | 0.744 |

In order to confirm the reduction processes, the electrochemical reduction of the bilayer nanographene **1** by cyclic and square wave voltammetry at room temperature, using toluene/acetonitrile (4:1) as solvent, was carried out. In agreement with the aforementioned experimental results, three reduction waves are observed at high negative values (−2.12; −2.30; −2.63 V) using $Fc/Fc^+$ as reference electrode. The first and second reduction potentials appear at close values as a broad wave with two distinguishable reduction peaks (see Figure S7 in the Supporting Information). However, whereas the second and third reduction waves are quasi-reversible, the first one appears as an irreversible one.

Density Functional Theory (DFT) calculations were carried out at the dispersion-corrected B3LYP-D3/def2-SVP level (see computational details in the Supporting Information) to gain more insight into the formation of the radical-trianion ($C_{138}H_{122}^{3-}$) from the bilayer nanographene **1** ($C_{138}H_{120}$). To this end, we focused on a model compound **1M**, where the bulky *t*-butyl groups in **1** were replaced by methyl groups.

Figure 7 shows that the LUMO of **1M**, i.e. the orbital accepting the first electron from the alkali metal upon reduction, can be viewed as a π*-molecular orbital located exclusively in the helicene moiety. As a consequence, the unpaired electron in the readily formed radical anion $\mathbf{1M}^{\bullet-}$ is localized in the helicene fragment, and particularly at the carbon atoms located on the edge of the helicene backbone (see computed spin densities in Figure 7). Therefore, the subsequent hydrogenation reaction, which very likely occurs through a $H^\bullet$ abstraction from the water entrapped in the cavities of bilayer nanographene structure, should occur preferentially at these positions leading to the hydrogenated anionic $\mathbf{1M–H}^-$ intermediate. Once the formation of the hydrogenated monoanion $\mathbf{1M–H}^-$ has occurred, a new reduction/H-abstraction process occurs leading to the formation of the dianion $\mathbf{1M–2H}^{2-}$. The site-specific hydrogenation, in this case, becomes even more evident upon simple visual inspection of the LUMO of monoanion $\mathbf{1M–H}^-$, which is almost exclusively localized on the edge carbon atom of the non-hydrogenated helicene moiety. Not surprisingly, the LUMO of this species is also delocalized within the carbon atom located in relative *para*-position as a consequence of π-conjugation, a situation also occurring in the initial nanographene **1M** and the radical-anion $\mathbf{1M}^{\bullet-}$. Therefore, our calculations suggest that the complete site-specific hydrogenation observed experimentally finds its origin in the localization of the unpaired electrons on the edge carbon atoms of the helicene fragment of nanographene **1**.

Once the dianion $\mathbf{1M–2H}^{2-}$ is formed, a new reduction process takes place leading to the formation of the radical trianion $\mathbf{1M–2H}^{\bullet3-}$. At variance with the previous anions $\mathbf{1M–H}^{\bullet-}$ or $\mathbf{1M–H}^{\bullet2-}$, on this occasion the new unpaired electron is not localized on the edge carbon atoms of the helicene (which are now hydrogenated) but clearly delocalized on the periphery of both HBC moieties. This delocalization precludes a further site-specific hydrogenation step and for this reason, only two hydrogen atoms can be incorporated during the reduction process.

Finally, we also computed the maps of electrostatic potential (MEP) of the key species involved in the reduction/hydrogenation process. As shown in Figure 7, the negative charges in dianion $\mathbf{1M–2H}^{2-}$ and radical trianion $\mathbf{1M–2H}^{\bullet3-}$ (as well as in monoanionic $\mathbf{1M–H}^-$) are spread over both HBC moieties and, particularly, over the six-membered rings closer to the helicene tether. This is consistent with i) the observed slippage of the HBC layers as a consequence of the increased electronic repulsion and ii) the coordination of the alkali metal ions to these positions, as shown above for the Rb complex **3** (see Figures 4 and 5). Different binding preferences of potassium and rubidium cations observed in **2** and **3** could be related to their different ionic size, and similar differences have been previously reported.[25b,26] This hypothesis is supported by the lack of formation of related crystals involving the smaller $Li^+$-cations.

Interestingly, despite the slippage of the HBC layers induced by the reduction-hydrogenation process, the stabilizing π–π interaction present in the initial nanographene **1** is preserved in the final radical trianion. This can be easily visualized by means of the NCIPLOT method,[27] which clearly shows the occurrence of a significant noncovalent attractive interaction (green surface in Figure 8) between the aromatic rings of both HBC moieties either in **1M** or in $\mathbf{1M–2H}^{\bullet3-}$. As a consequence, the rare AA arrangement exhibited by **1**, where the two HBC layers becomes almost parallel, is also preserved in the isolated radical trianions **2** and **3**.

## Conclusion

In summary, the chemical reduction of bilayer nanographene **1** ($C_{138}H_{120}$) with K and Rb metals afforded two new products that were characterized crystallographically as $[K^+(18\text{-crown-6})(THF)_2][\{K^+(18\text{-crown-6})\}_2(THF)_{0.5}][C_{138}H_{122}^{3-}]$ (**2**) and $[Rb^+(18\text{-crown-6})_2][\{Rb^+(18\text{-crown-6})\}_2(C_{138}H_{122}^{3-})]$ (**3**). The formation of the new radical trianion, which incorporated two hydrogen atoms in the helical framework, very likely takes place by stepwise chemical reduction of the bilayer nanographene **1** affording three different reduced states with one, two, and three electrons added to the π-conjugated network in **1**. Interestingly, the computational results reveal that the localization of the first two electrons in the helicene moiety is mainly responsible for this unprecedented site-specific hydrogenation process observed (and this is also confirmed by $^1H$ NMR spectroscopy data). Furthermore, the X-ray structure determination of a radical trianion ($\mathbf{1}^{\bullet3-}$) is not common and it could be accounted for by the delocalization undergone by the third electron on the periphery of both HBC moieties. Since the negative charges are spread over both HBC moieties, and, particularly, over the six-membered rings closer to the helicene tether, coordination of the alkali metal ions to these positions accounts for the Rb(I) complex **3** and also for the observed slippage of the HBC layers as a result of the increased electronic density within them. Despite that, the stabilizing π–π interaction present in the initial nanographene **1** is

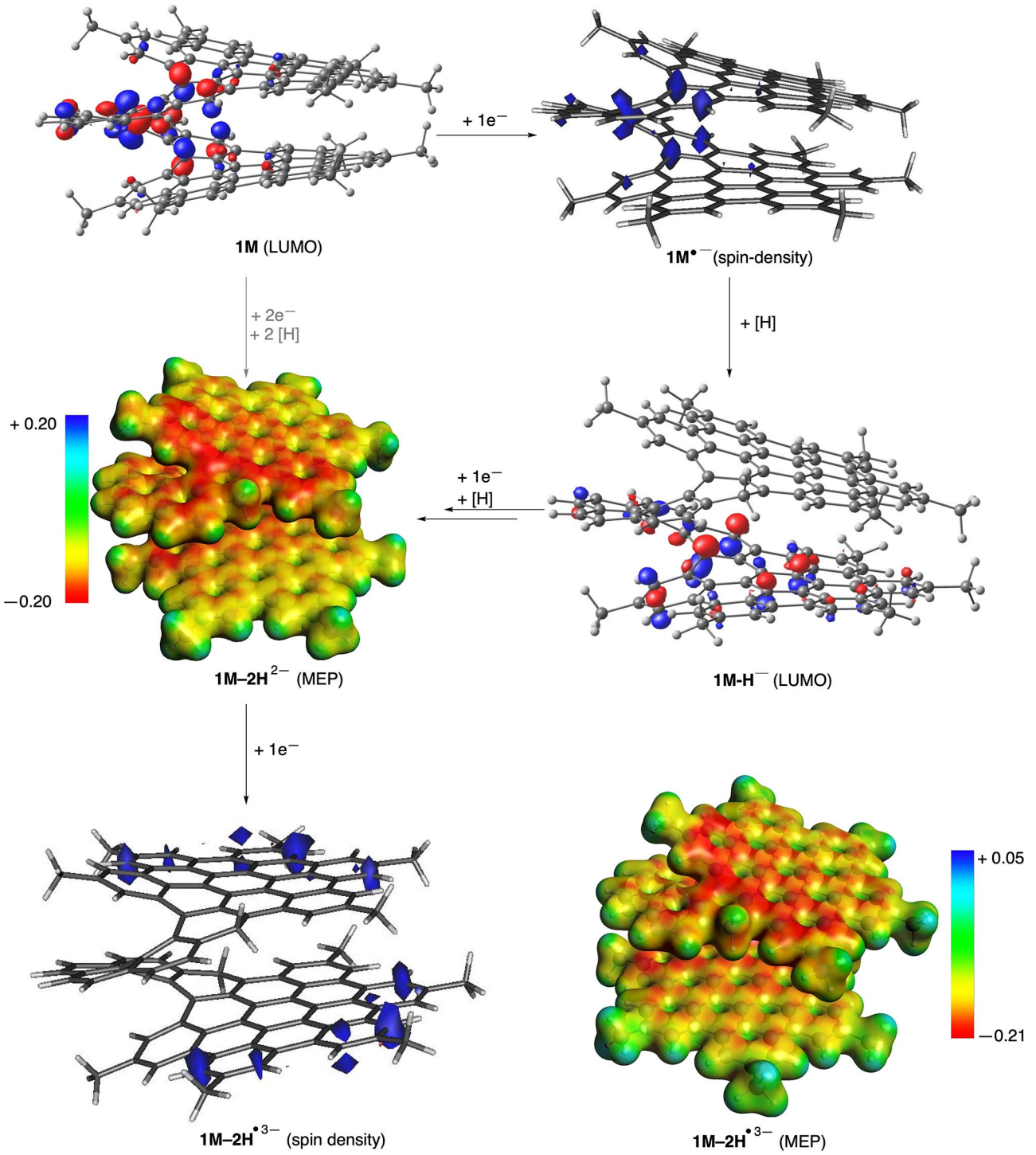


***Figure 7.*** Computed key species for reduction-induced hydrogenation of helical bilayer nanographene **1M**. All data have been computed at the B3LYP-D3/def2-SVP level.

preserved in the final radical-trianion, as so is the rare AA arrangement of these species.

These new reduction-induced hydrogenation results represent one step further in the understanding of the chemical reactivity of π-extended helicenes and pave the way to further site-selective chemical reactions. Furthermore, the coordination observed for $Rb^+$ cations opens a new scenario for the preparation, in a selective manner, of new organometallic species from less-explored molecular nanographenes.[28]

Finally, since molecular nanographenes exhibit a variety of amazing chemical, photophysical, electrochemical, imaging, sensing and/or chiroptical properties, the data now reported open new opportunities for these chemically

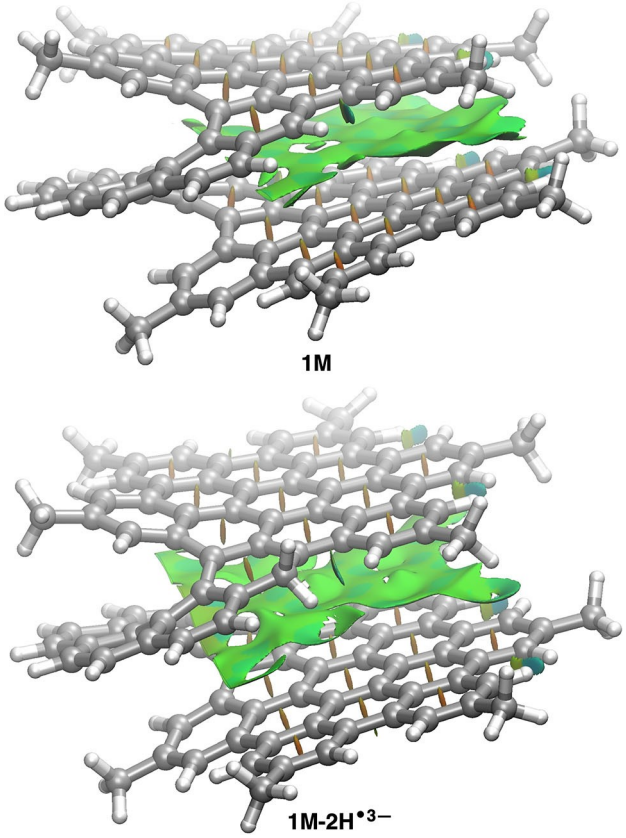


***Figure 8.*** Contour plots of the reduced density gradient isosurfaces (density cutoff of 0.045 a.u.) for compound **1M** (top) and radical trianion **1M–2H**$^{\bullet 3-}$ (bottom). The green surfaces indicate attractive noncovalent interactions.

modified carbon-based molecular nanostructures. Further work on this regard is being currently carried out in our laboratories.

## Acknowledgements

Financial support of this work from the U. S. National Science Foundation, CHE-2003411, is acknowledged by M. A. P. NSF's ChemMatCARS Sector 15 is principally supported by the Divisions of Chemistry (CHE) and Materials Research (DMR), National Science Foundation, under grant number NSF/CHE-1834750. The use of the Advanced Photon Source, an Office of Science User Facility operated for the U.S. Department of Energy (DOE) Office of Science by Argonne National Laboratory, was supported by the U.S. DOE under Contract No. DE-AC02-06CH11357. Financial support from the Spanish MICINN (Projects PID2020-114653RB-I00 and RED2018-102815-T to N.M. and PID2019-106184GB-I00 and RED2018-102387-T to I.F.). R.R. thanks Xunta de Galicia for a Postdoctoral fellowship. J.C. thanks the the Ministère de l'Education Nationale, de la Recherche et de la Technologie and the Centre National de la Recherche Scientifique (CNRS).

## Conflict of Interest

The authors declare no conflict of interest.

## Data Availability Statement

The data that support the findings of this study are available from the corresponding author upon reasonable request.

**Keywords:** Chemical reduction · DFT calculations · Helical bilayer · Hydrogenation · X-ray crystallography

[1] a) K. S. Novoselov, A. K. Geim, S. V. Morozov, D. Jiang, Y. Zhang, S. V. Dubonos, I. V. Grigorieva, A. A. Firsov, *Science* **2004**, *306*, 666–669; b) A. K. Geim, K. S. Novoselov, *Nat. Mater.* **2007**, *6*, 183–191.

[2] a) K. S. Novoselov, V. I. Fal'ko, L. Colombo, P. R. Gellert, M. G. Schwab, K. Kim, *Nature* **2012**, *490*, 192–200; b) G. Bottari, M. Á. Herranz, L. Wibmer, M. Volland, L. Rodríguez-Pérez, D. M. Guldi, A. Hirsch, N. Martín, F. D'Souza, T. Torres, *Chem. Soc. Rev.* **2017**, *46*, 4464–4500; c) N. Martín, N. Tagmatarchis, Q. H. Wang, X. Zhang, *Chem. Eur. J.* **2020**, *26*, 6292–6295.

[3] a) J. Liu, X. Feng, *Angew. Chem. Int. Ed.* **2020**, *59*, 23386–23401; *Angew. Chem.* **2020**, *132*, 23591–23607; b) Z. Sun, S. Fang, Y. H. Hu, *Chem. Rev.* **2020**, *120*, 10336–10453.

[4] a) F. Bonaccorso, Z. Sun, T. Hasan, A. Ferrari, *Nat. Photonics* **2010**, *4*, 611–622; b) C. Wang, H. Dong, W. Hu, Y. Liu, D. Zhu, *Chem. Rev.* **2012**, *112*, 2208–2267; c) R. M. Metzger, *Chem. Rev.* **2015**, *115*, 5056–5115; d) N. Martín, *Adv. Energy Mater.* **2017**, *7*, 1601102.

[5] a) A. Sánchez-Grande, J. I. Urgel, A. Cahlík, J. Santos, S. Edalatmanesh, E. Rodríguez-Sánchez, K. Lauwaet, P. Mutombo, D. Nachtigallová, R. Nieman, H. Lischka, B. de la Torre, R. Miranda, O. Gröning, N. Martín, P. Jelínek, D. Écija, *Angew. Chem. Int. Ed.* **2020**, *59*, 17594–17599; *Angew. Chem.* **2020**, *132*, 17747–17752; b) Q. Sun, Y. Yan, X. Yao, K. Müllen, A. Narita, R. Fasel, P. Ruffieux, *J. Phys. Chem. Lett.* **2021**, *12*, 8679–8684.

[6] a) A. Narita, X.-Y. Wang, X. Feng, K. Müllen, *Chem. Soc. Rev.* **2015**, *44*, 6616–6643; b) M. Stępien, E. Gonk´a, M. Żyła, N. Sprutta, *Chem. Rev.* **2017**, *117*, 3479–3716; c) I. Pozo, E. Guitián, D. Pérez, D. Peña, *Acc. Chem. Res.* **2019**, *52*, 2472–2481.

[7] a) Y. R. Kumar, K. Deshmukh, K. K. Sadasivuni, S. K. K. Pasha, *RSC Adv.* **2020**, *10*, 23861–23898; b) M. Vázquez-Nakagawa, L. Rodríguez-Pérez, M. Á. Herranz, N. Martín, *Chem. Commun.* **2016**, *52*, 665–668; c) C. I. M. Santos, L. Rodríguez-Pérez, G. Gonçalves, S. N. Pinto, M. Melle-Franco, P. A. A. P. Marques, M. A. F. Faustino, M. A. Herranz, N. Martín, M. G. P. M. S. Neves, J. M. G. Martinho, E. M. S. Maçôas, *Carbon* **2020**, *166*, 164–174.

[8] a) X.-Y. Wang, A. Narita, K. Müllen, *Nat. Chem. Rev.* **2018**, *2*, 100–112; b) Y. Segawa, H. Ito, K. Itami, *Nat. Rev. Mater.* **2016**, *1*, 15002; c) H. Ito, K. Ozaki, K. Itami, *Angew. Chem. Int. Ed.* **2017**, *56*, 11144–11164; *Angew. Chem.* **2017**, *129*, 11296–11317; d) H. Zhylitskaya, M. Stępien, *Org. Chem. Front.* **2018**, *5*, 2395–2414; e) J. M. Fernández-García, P. J. Evans, S. Medina Rivero, I. Fernández, D. García-Fresnadillo, J. Perles, J. Casado, N. Martín, *J. Am. Chem. Soc.* **2018**, *140*, 17188–17196.

[9] a) J. M. Fernández-García, P. J. Evans, S. Filippone, M. A. Herranz, N. Martín, *Acc. Chem. Res.* **2019**, *52*, 1565–1574; b) B. Zhao, S. Yang, J. Deng, K. Pan, *Adv. Sci.* **2021**, *8*, 2003681;

c) S. Nishitani, R. Sekiya, T. Haino, *Angew. Chem. Int. Ed.* **2020**, *59*, 669–673; *Angew. Chem.* **2020**, *132*, 679–683; d) P. Izquierdo-García, J. M. Fernández-García, I. Fernández, J. Perles, N. Martín, *J. Am. Chem. Soc.* **2021**, *143*, 11864–11870.

[10] a) J. Urieta-Mora, M. Krug, W. Alex, J. Perles, I. Fernández, A. Molina-Ontoria, D. M. Guldi, N. Martín, *J. Am. Chem. Soc.* **2020**, *142*, 4162–4172; b) S. Mishra, D. Beyer, K. Eimre, S. Kezilebieke, R. Berger, O. Groning, C. A. Pignedoli, K. Müllen, P. Liljeroth, P. Ruffieux, X. Feng, R. Fasel, *Nat. Nanotechnol.* **2020**, *15*, 22–28; c) L. Đorđević, C. Valentini, N. Demitri, C. Mézière, M. Allain, M. Sallé, A. Folli, D. Murphy, S. Mañas-Valero, E. Coronado, D. Bonifazi, *Angew. Chem. Int. Ed.* **2020**, *59*, 4106–4114; *Angew. Chem.* **2020**, *132*, 4135–4143.

[11] a) J. Cao, Y. M. Liu, X. Jing, J. Yin, J. Li, B. Xu, Y. Z. Tan, N. Zheng, *J. Am. Chem. Soc.* **2015**, *137*, 10914–10917; b) Y.-M. Liu, H. Hou, Y.-Z. Zhou, Z.-J. Zhao, C. Tang, Y.-Z. Tan, K. Müllen, *Nat. Commun.* **2018**, *9*, 1901; c) M. C. Stuparu, *Acc. Chem. Res.* **2021**, *54*, 2858–2870.

[12] a) H.-J. Yen, H. Tsai, M. Zhou, E. F. Holby, S. Choudhury, A. Chen, L. Adamska, S. Tretiak, T. Sánchez, H. Iyer Zhang, L. Zhu, H. Lin, L. Dai, G. Wu, H.-L. Wang, *Adv. Mater.* **2016**, *28*, 10250–10256; b) A. V. Zabula, S. N. Spisak, A. S. Filatov, A. Yu Rogachev, M. A. Petrukhina, *Acc. Chem. Res.* **2018**, *51*, 1541–1549; c) Y. Zhang, Y. Zhu, D. Lan, S. H. Pun, Z. Zhou, Z. Wei, Y. Wang, H. K. Lee, C. Lin, J. Wang, M. A. Petrukhina, Q. Li, Q. Miao, *J. Am. Chem. Soc.* **2021**, *143*, 5231–5238; d) A. Yu Rogachev, Z. Zhou, S. Liu, Z. Wei, T. A. Schaub, R. Jasti, M. A. Petrukhina, *Chem. Sci.* **2021**, *12*, 6526–6535.

[13] a) N. Panwar, A. M. Soehartono, K. K. Chan, S. Zeng, G. Xu, J. Qu, P. Coquet, K. T. Yong, X. Chen, *Chem. Rev.* **2019**, *119*, 9559–9656; b) E. Jin, Q. Yang, C. W. Ju, Q. Chen, K. Landfester, M. Bonn, K. Müllen, X. Liu, A. Narita, *J. Am. Chem. Soc.* **2021**, *143*, 10403–10412.

[14] P. J. Evans, J. Ouyang, L. Favereau, J. Crassous, I. Fernández, J. Perles, N. Martín, *Angew. Chem. Int. Ed.* **2018**, *57*, 6774–6779; *Angew. Chem.* **2018**, *130*, 6890–6895.

[15] a) M. Milton, N. J. Schuster, D. W. Paley, R. Hernandez Sanchez, F. Ng, M. L. Steigerwald, C. Nuckolls, *Chem. Sci.* **2019**, *10*, 1029–1034; b) X. J. Zhao, H. Hou, X. T. Fan, Y. Wang, Y. M. Liu, C. Tang, S. H. Liu, P. P. Ding, J. Cheng, D. H. Lin, C. Wang, Y. Yang, Y. Z. Tan, *Nat. Commun.* **2019**, *10*, 3057; c) X. J. Zhao, H. Hou, P. P. Ding, Z. Y. Deng, Y. Y. Ju, S. H. Liu, Y. M. Liu, C. Tang, L. B. Feng, Y. Z. Tan, *Sci. Adv.* **2020**, *6*, eaay8541.

[16] R. Quhe, J. Ma, Z. Zeng, K. Tang, J. Zheng, Y. Wang, Z. Ni, L. Wang, Z. Gao, J. Shi, J. Lu, *Sci. Rep.* **2013**, *3*, 2289.

[17] L. Banszerus, B. Frohn, T. Fabian, S. Somanchi, A. Epping, M. Müller, D. Neumaier, K. Watanabe, T. Taniguchi, F. Libisch, B. Beschoten, F. Hassler, C. Stampfe, *Phys. Rev. Lett.* **2020**, *124*, 177701.

[18] L. Ju, L. Wang, T. Cao, T. Taniguchi, K. Watanabe, S. G. Louie, F. Rana, J. Park, J. Hone, F. Wang, P. L. McEuen, *Science* **2017**, *358*, 907–910.

[19] a) M. Eich, R. Pisoni, A. Pally, H. Overweg, A. Kurzmann, Y. Lee, P. Rickhaus, K. Watanabe, T. Taniguchi, K. Esslin, T. Ihn, *Nano Lett.* **2018**, *18*, 5042–5048; b) J. Lu, A. Lipatov, N. S. Vorobeva, D. S. Muratov, A. Sinitskii, *Adv. Electron. Mater.* **2018**, *4*, 1800021; c) Y. Saito, J. Ge, K. Watanabe, T. Taniguchi, A. F. Young, *Nat. Phys.* **2020**, *16*, 926–930.

[20] Y. Cao, V. Fatemi, S. Fang, K. Watanabe, T. Taniguchi, E. Kaxiras, P. Jarillo-Herrero, *Nature* **2018**, *556*, 43–50.

[21] a) M. Kühne, F. Börrnert, S. Fecher, M. Ghorbani-Asl, J. Biskupek, D. Samuelis, A. V. Krasheninnikov, U. Kaiser, J. H. Smet, *Nature* **2018**, *564*, 234–239; b) K. Ji, J. Han, A. Hirata, T. Fujita, Y. Shen, S. Ning, P. Liu, H. Kashani, Y. Tian, Y. Ito, J.-i. Fujita, Y. Oyama, *Nat. Commun.* **2019**, *10*, 275.

[22] H. Chen, S. Gui, Y. Zhang, Z. Liu, Q. Miao, *CCS Chem.* **2021**, *3*, 613–619.

[23] a) A. V. Zabula, S. N. Spisak, A. S. Filatov, V. M. Grigoryants, M. A. Petrukhina, *Chem. Eur. J.* **2012**, *18*, 6476–6484; b) S. N. Spisak, Z. Wei, E. Darzi, R. Jasti, M. A. Petrukhina, *Chem. Commun.* **2018**, *54*, 7818–7821; c) Z. Zhou, R. K. Kawade, Z. Wei, F. Kuriakose, Ö. Üngör, M. Jo, M. Shatruk, R. Gershoni-Poranne, M. A. Petrukhina, I. V. Alabugin, *Angew. Chem. Int. Ed.* **2020**, *59*, 1256–1262; *Angew. Chem.* **2020**, *132*, 1272–1278; d) Z. Zhou, Z. Wei, T. Hirao, T. Amaya, M. A. Petrukhina, *Organometallics* **2021**, *40*, 2023–2026.

[24] Deposition Numbers 2114475 (for **2**) and 2114476 (for **3**) contain the supplementary crystallographic data for this paper. These data are provided free of charge by the joint Cambridge Crystallographic Data Centre and Fachinformationszentrum Karlsruhe Access Structures service www.ccdc.cam.ac.uk/structures.

[25] a) Z. Zhou, S. N. Spisak, Q. Xu, A. Yu Rogachev, Z. Wei, M. Marcaccio, M. A. Petrukhina, *Chem. Eur. J.* **2018**, *24*, 3455–3463; b) Z. Zhou, L. Fu, Y. Hu, X. Y. Wang, Z. Wei, A. Narita, K. Müllen, M. A. Petrukhina, *Angew. Chem. Int. Ed.* **2020**, *59*, 15923–15927; *Angew. Chem.* **2020**, *132*, 16057–16061.

[26] a) S. N. Spisak, N. J. Sumner, A. V. Zabula, A. S. Filatov, A. Yu Rogachev, M. A. Petrukhina, *Organometallics* **2013**, *32*, 3773–3779; b) A. Yu Rogachev, Y. Zhu, Z. Zhou, S. Liu, Z. Wei, M. A. Petrukhina, *Org. Chem. Front.* **2020**, *7*, 3591–3598.

[27] E. R. Johnson, S. Keinan, P. Mori-Sánchez, J. Contreras-García, A. J. Cohen, W. Yang, *J. Am. Chem. Soc.* **2010**, *132*, 6498–2506.

[28] a) T. Wombacher, R. Goddard, C. W. Lehmann, J. J. Schneider, *Chem. Commun.* **2017**, *53*, 7030–7033; b) T. Wombacher, R. Goddard, C. W. Lehmann, J. J. Schneider, *Dalton Trans.* **2018**, *47*, 10874–10883.

Manuscript received: November 18, 2021
Accepted manuscript online: December 7, 2021
Version of record online: ■■, ■■

# Research Articles

## Nanomaterials

Z. Zhou, J. M. Fernández-García, Y. Zhu, P. J. Evans, R. Rodríguez, J. Crassous, Z. Wei, I. Fernández,* M. A. Petrukhina,* N. Martín* e202115747

Site-Specific Reduction-Induced Hydrogenation of a Helical Bilayer Nanographene with K and Rb Metals: Electron Multiaddition and Selective $Rb^+$ Complexation

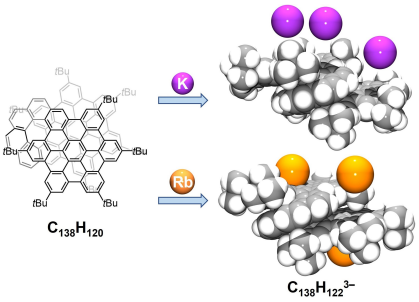


An unprecedented site-specific reduction-induced hydrogenation of a helical bilayer nanographene has been found using K or Rb metals. However, coordination of the metal to the central six-membered rings of the bilayer helicene in a $\eta^3$-mode is only observed for the Rb complex, due to its larger ionic size, thus showing the impact of the cation's size on the reaction product.